Interfacial Assembly of Bacterial Microcompartment Shell Proteins in Aqueous Multi-phase Systems

A. A. Dharani T. Abeysinghe[1,#], Eric J. Young[2,3,#], Andrew T. Rowland[1], Lucas C. Dunshee[4,5], Sandeep Urandur[4,5], Millicent O. Sullivan[4,5], Cheryl A. Kerfeld [2,3,6,7*], and Christine D. Keating[1*]

[1]Department of Chemistry, Pennsylvania State University

[2]Environmental Genomics and Systems Biology Division, Lawrence Berkeley National Laboratory, Berkeley, CA, USA

[3]Department of Biochemistry and Molecular Biology, Michigan State University, East Lansing, MI, USA

[4]Department of Chemical and Biomolecular Engineering, University of Delaware

[5]Department of Biomedical Engineering, University of Delaware

[6]Molecular Biophysics and Integrated Bioimaging Division, Lawrence Berkeley National Laboratory, Berkeley, CA, USA

[7]MSU-DOE Plant Research Laboratory, Michigan State University, East Lansing, MI, USA

#Co-first Authors

*Co-corresponding Authors

Keywords

Synthetic Cell; Protocell; Compartmentalization; Self-assembly; Bioreactor; Bottom-up Synthetic Biology

Abstract

Compartments are a fundamental feature of life, based variously on lipid membranes, protein shells, or biopolymer phase separation. Here, we combine self-assembling bacterial microcompartment (BMC) shell proteins and liquid-liquid phase separation (LLPS) to develop new forms of compartmentalization. We found that BMC shell proteins assemble at the liquid-liquid interfaces between either (1) the dextran-rich droplets and PEG-rich continuous phase of a poly(ethyleneglycol)(PEG)/dextran aqueous two-phase system, or (2) the polypeptide-rich coacervate droplets and continuous dilute phase of a polylysine/polyaspartate complex coacervate system. Interfacial protein assemblies in the coacervate system were sensitive to the ratio of cationic to anionic polypeptides, consistent with electrostatically-driven assembly. In

both systems, interfacial protein assembly competed with aggregation, with protein concentration and polycation availability impacting coatings. These two LLPS systems were then combined to form a three-phase system wherein coacervate droplets were contained within dextran-rich phase droplets. Interfacial localization of BMC hexamer shell proteins was tunable in a three-phase system through changing the polyelectrolyte charge ratio. The tens-of-micron scale BMC shell protein coated droplets introduced here can accommodate bioactive cargo such as enzymes or RNA and represent a new synthetic cell strategy for organizing biomimetic functionality.

Introduction

The compartmentalization of molecules to form protocells is considered a key step in the emergence of life.[1,2] Cellular and subcellular compartments provide spatially and chemically distinct microenvironments important for the organization of life-sustaining processes. In addition to long-recognized phospholipid membrane-based compartment organelles, such as the nucleus and mitochondria, other subcellular compartments include membraneless organelles formed by liquid-liquid phase separation (LLPS) and megadalton-sized protein-based metabolic microcompartments.[3–5] Bottom-up synthetic biology approaches inspired by each of these natural forms of compartmentalization have been produced in the pursuit of understanding early life, designing novel bioreactors, and generating protocells with increasingly complex, lifelike properties.[6–9] Building lipid-based compartments has received the most attention to-date, resulting in "cell-sized" compartments that take advantage of the barrier properties of lipid membranes.[10,11] LLPS has also been harnessed to create macromolecularly-crowded, "cytoplasm-like" droplets that contain distinct interior physio-chemical microenvironments amenable to loading with biomolecular cargo, such as enzymes and nucleic acids, but lack a definitive membrane-like boundary layer.[4,12,13] Protein-based bacterial microcompartments (BMCs), ranging from 40 nm to hundreds of nanometers in size, provide another strategy for building self-assembled structures that have a protein-based selectively permeable shell that functions as a membrane.[5,14] Inspired by the versatile and complementary properties of distinct compartment-types such as LLPS droplets and BMCs, we sought to explore whether LLPS droplets and BMC shell proteins could be combined as a new type of synthetic cell.

BMC shell proteins are conserved across functionally distinct BMCs. Two types, tiles named: BMC-H proteins[15] and BMC-T proteins,[16] form hexagonal tiles. BMC-P proteins assemble into pentagonal oligomers.[17] Some BMC shell proteins, when heterologously expressed or mixed together in aqueous buffered solution, assemble into empty shells.[18–25] In general, empty synthetic compartments are typically ~40 nm or less with a few exceptions.[26,27] Larger compartments (~600 nm) have been produced by Bari et al. by templating BMC shell protein assembly around an aqueous-in-oil droplet.[28] Additionally, theoretical and computational efforts suggest that interior cargos, along with a tile's intrinsic preference for a tile-tile curvature angle, influences the size, shape, and productive assembly of compartments.[29–31] This suggests overall that combining BMC shell proteins with other biocompatible droplet templating strategies may be valuable in constructing micron-scale protein-bound cell-like compartments.

All-aqueous systems such as aqueous two-phase systems (ATPS) and coacervates can provide microscale droplets as templates for assembly. Such droplets have been coated with various molecular and particulate layers, often in an attempt to stabilize droplets by preventing coalescence, which otherwise generally occurs following droplet contact.[32–36] For example, lipid membranes,[37–39] nano and microparticles,[40–42] block copolymers and peptides,[43–45] other synthetic or natural polymers such as polysaccharides and proteins,[35,46,47] and even living biological cells[48] have coated droplets. Protein-based coatings are of special interest because of their structural and functional diversity and because the properties of proteins are directly encodable. Droplet coatings have included non-specifically aggregated proteins,[49] covalently cross-linked protein/polymer conjugates,[35,50–52] and higher-order oligomeric protein structures such as filaments and fibers.[53–55] Templating protein "membranes" around LLPS droplets enables control of a droplet's size, shape, permeability, and stability.[54–56] Depending on the type of all-aqueous LLPS, interfacial absorption and templating of proteins can rely on interface volume availability or charge-specific interactions between the droplet and protein.[35,52]

Here, we explore using all-aqueous LLPS droplets to template BMC-H shell proteins, which self-assemble into 2-D lattices[18,21] as a methodology to create tens-of-micron sized structures that represent a novel form of protein-membrane bound synthetic cell chassis **(Figure 1)**. Two representative LLPS systems were studied: (1) PEG and dextran aqueous two-phase system

(ATPS)[34,57,58] as an example of a non-associative system, and (2) polylysine/polyaspartate coacervates as an example of an associative system, specifically complex coacervation.[59,60] We find labeled shell proteins at the interface in both PEG/dextran and coacervate systems. Electrostatic interactions play a key role in modulating interfacial partitioning in coacervate droplets, whereas shell protein assembly influences partitioning in both systems. By combining the PEG/dextran ATPS and polypeptide coacervate systems, nested organelle-like coacervate droplets were produced within larger, dextran-rich phase droplets. Shell protein coatings could be formed either around the coacervates or at the dextran/exterior boundary by choice of polyelectrolyte charge ratio. LLPS droplet templating of BMC shell proteins formed tens of micron-scale synthetic compartments containing bioactive cargos and engineerable shell protein droplet coatings based on LLPS droplet composition.

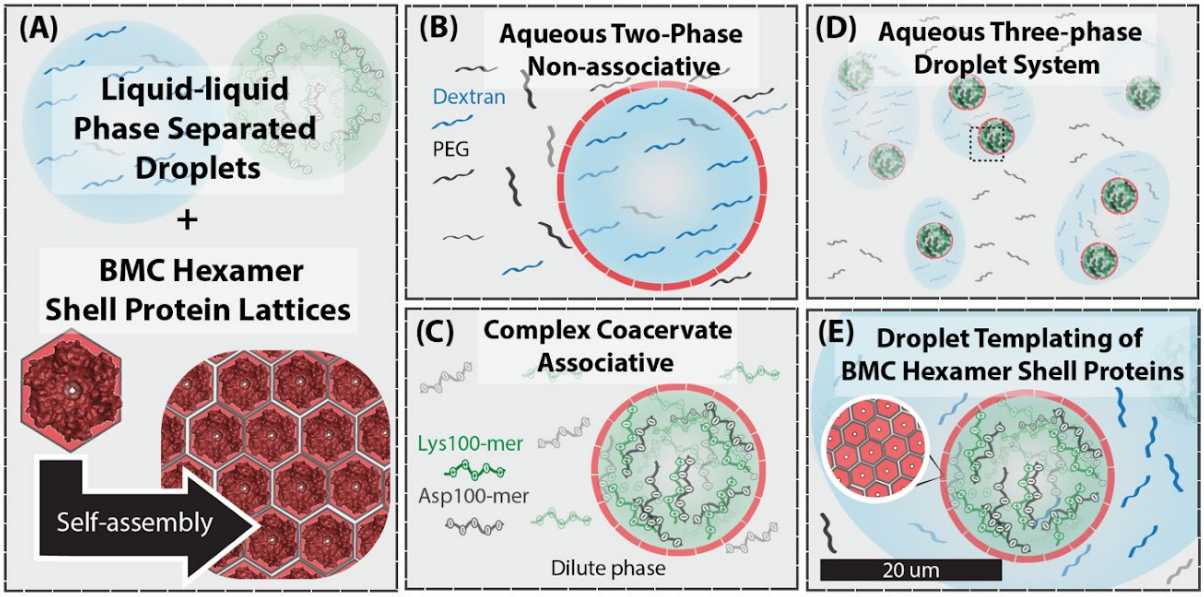

Figure 1: Micron-scale BMC shell protein coated compartments templated at aqueous/aqueous interfaces. (A) General strategy of mixing liquid-liquid phase separated droplets with BMC-H shell proteins that self-assemble into lattices to form BMC-H shell protein "membranes" around the droplets. (B) – (D) Experimental systems used for interfacial protein assembly. (E) Model of interface assembly of BMC-H proteins templated on a coacervate nested within a non-associative phase droplet system.

Results and Discussion:

Characterization of fluorescently labeled BMC shell proteins for coating LLPS droplets.

We selected a BMC-H protein known to avidly self-assemble into 2-D sheets, as well as its single amino acid substitution derivative, K28A, to study BMC shell protein assembly when mixed with polymer-rich droplets **(Figure 1)**.[18,21,61] The native BMC-H (hereafter BMC-H_{wt}) and BMC-H_{K28A} form single or double layer sheets on carbon supports, respectively.[21] Purified BMC-H_{wt} and BMC-H_{K28A} shell protein stocks of approximately 100 mg/ml were prepared using heterologous overexpression and protein purification (see **Methods**). The purified protein was covalently labeled with amine reactive NHS-ester Sulfo-Cy3. Fluorophore labeling did not affect the rheoscopic appearance of shell protein solutions. **(Fig. Sup. 1)**. Transmission electron microscopy (TEM) further supported that Sulfo-Cy3 dye conjugation did not disrupt higher-order self-assembly of labeled hexamers (**Fig. Sup. 2**).

BMC shell protein assembly in a PEG/dextran ATPS system.

We chose the well-characterized PEG 8kDa/dextran 10kDa ATPS to study the assembly behavior of the shell proteins with a non-associative phase separating neutral polymers system. This system forms two macromolecularly-crowded phases, one enriched in PEG and the other in dextran.[57] Assembly of amphiphilic molecules (*e.g.* phospholipids, block copolymers, surfactant-like proteins) to form coatings around droplets has been reported at PEG/dextran interfaces.[39,43,62] Interfacial protein assembly has also been reported when proteins are present as larger aggregates, which behave similarly to other particulates (*e.g.* ~100 nm lipid vesicles, mineral microparticles).[49,53,63–66] Interfacial assembly at other liquid-liquid interfaces (e.g., oil/water) is generally viewed as a result of favorable removal of interfacial area with the energy to remove an adsorbed particle, $\Delta E = \pi r^2 \gamma [1-|\cos\theta|)^2$, where r is the radius for a spherical particle, γ is the interfacial tension between the two liquid phases, and θ is the contact angle describing how the particle is wet by the phases.[67–69] Since ATPS have low interfacial tensions (~1 to 100s of mN/m), appreciable interfacial accumulation for objects as small as individual BMC shell protein hexamers (~7 nm diameter) is unlikely at room temperature.[65,70,71] Nonetheless, when Cy3-labeled BMC-H shell proteins (~0.1 mg/mL) were mixed with a PEG/dextran ATPS at a volume ratio of 9:1 (see **Methods**), some protein accumulation was seen at the interface between the PEG-rich and dextran-rich phases, coating ~40% of the interface as

estimated from the in-focus portion visible in confocal fluorescence images **(Figure 2, Sup. Fig. 3A)**. In these portions, shell proteins were partitioned between the interface, PEG-rich phase and the dextran-rich phase at a ratio of ~ 17: 1: 1 respectively, based on fluorescence intensities **(Sup.Fig.6)**. BMC-H_{K28A} shell protein hexamers assembled similarly under these conditions (**Sup. Fig. 3B)**. These observations can be rationalized by considering that (i) anisotropic particle shapes such as the disk-like hexamers adsorb more strongly at the interface as compared to spheres of the same volume,[41,42,72] and (ii) the higher-order assembly propensity of the shell proteins further aids interfacial accumulation by increasing particle size. We also note that ATPS aqueous/aqueous interfaces differ from oil/water interfaces (where particle interface assembly is more traditionally studied) in their relative thickness, which is anticipated to be on the same scale as the phase components and hence much larger for the polymer-rich ATPS phases as compared to oil/water systems.[64,73] ATPS interfaces have been described as being depleted in both polymers,[64,66] potentially providing an additional mechanism for collection of nanoscale objects such as BMC shell proteins within this region, wherein macromolecular crowding from the PEG-rich and dextran-rich phases drives them to this interfacial region. Regardless of the energetic specifics of adsorption, we reasoned that the relatively sparse interfacial coatings observed in Figure 2 may reflect adsorption energies that are close to kT, or could be due to an insufficient quantity of shell protein. We therefore next increased the amount of shell protein in our experiments.

Addition of either BMC-H_{wt} or BMC-H_{K28A} shell proteins at higher concentration (~100 mg/mL) did not increase interfacial assembly, but instead led to large, three-dimensional protein aggregates that localized within the interior dextran-rich phase **(Sup. Fig. 3C-D)**. These data suggest that increased assembly of hexamers into larger structures was not limited to the interface and occurred in solution. Higher protein concentrations favor self-association, particularly in the presence of the PEG and dextran polymers, which are commonly used as macromolecular crowding agents.[74,75] At the polymer concentrations used herein, excluded volume effects can be expected to drive protein-protein association,[76] which could lead to not only the desired 2-dimensional, interfacial assemblies, but also the undesired 3-dimensional, solution-phase aggregates of the BMC shell proteins seen in **Sup Fig 3**. We also tested Sulfo-Cy3 labeling ratios and discovered that proteins with a lower density of Cy3 labeling appeared

within the dextran-rich phase and those labeled in an excess Cy3 label:shell protein ratio formed sparse interfacial assemblies **(Sup. Fig. 3E-F)**. Protein migration in an agarose gel supported the observation that increasing Cy3 label density decreased average size of macromolecular assemblies in solution **(Sup. Fig. 4)**. These data further suggest that protein assembly size and surface properties—dictated either by assembly state or density of fluorescent molecule labeling—influence the distribution of shell proteins in the PEG/dextran ATPS. Taken together, our results in PEG/dextran ATPS support the possibility of forming BMC shell protein coatings at the interface.

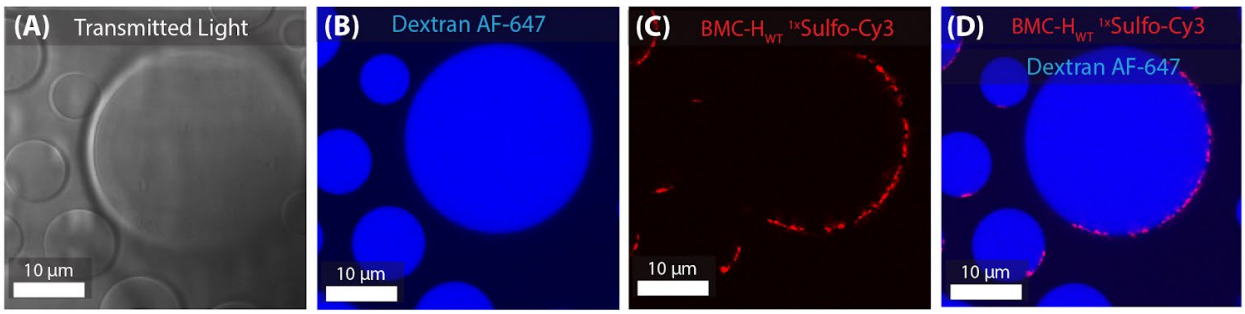

Figure 2: BMC-H$_{wt}$ proteins assemble into an incipient boundary layer at the aqueous/aqueous interface of PEG/dextran ATPS.

(A) - (D) Confocal fluorescence microscopy of Sulfo-Cy3-labeled BMC-H$_{wt}$ shell protein. (A) Transmitted light. (B) Dextran 10 kDa labeled with Alexa-647. (C) Sulfo-Cy3-labeled BMC-H$_{wt}$ shell protein. (D) Merged image. Fluorescence channels have been intensity-adjusted for ease of visualization and false-colored (blue for dextran 10kDa labeled with Alexa-647 and red for Sulfo-Cy3-labeled BMC-H$_{wt}$ shell proteins). Shell protein was added to a final concentration of ~0.1 mg/mL to a PEG 8kDa/dextran 10kDa ATPS (9:1 PEG-rich: dex-rich phase volume of an ATPS stock having 10 wt/wt% each polymer) in 20 mM Tris-HCl, 50 mM NaCl, 10 mM $MgCl_2$, pH 8.0 buffer. Images depicted represent trends observed for at least three biological replicates.

BMC shell protein assembly in K100/D100 coacervate systems.

Complex coacervation of oppositely charged polyelectrolytes produces polymer-rich coacervate phase droplets surrounded by a much larger and more dilute continuous phase.[77] Here, coacervates were prepared by mixing poly(lysine) 100-mers (K100) and poly(aspartate) 100-mers (D100) at 1:1 charge ratio and 5 mM charge concentration (where charge concentration =

charge per molecule x concentration; corresponding molecular concentrations are 0.05 mM K100, 0.05 mM D100). Sulfo-Cy3-labeled BMC shell proteins added to these coacervates adsorbed at the interface between the coacervate droplets (labeled by D100-AlexaFluor488; green) and the dilute continuous phase (**Figure 3A**). Coating assembly appeared more complete and uniform across this interface as compared to the PEG/dextran ATPS interface and the shell proteins were partitioned between the interface, dilute phase and the coacervate phase at a ratio of ~17:1:1.6, based on fluorescence intensities **(Sup. Fig.6)**. Possible explanations for this change in interfacial protein coatings in the coacervate system include differences in total interfacial area, interfacial tension, and/or assembly mechanism.[78]

We hypothesized that the assembly mechanism may differ for complex coacervates as compared with the PEG/dextran ATPS due to the possibility of charge-based interactions with the proteins in the K100/D100 system. Zeta potential measurements of the 1:1 K100/D100 coacervate droplets indicated that they were positively charged (+19 ± 1 mV), suggesting that favorable electrostatic interactions were occurring between the coacervate droplets and the negative charged BMC shell proteins (pI = 6.07, 5.59, pH = 8.0) **(Sup. Fig. 2)**. To test the effect of coacervate surface charge on the shell protein coating process, we changed the K100:D100 molecular ratio to favor either the polyanionic or the polycationic component and then examined the assembly behavior of the labeled BMC proteins at each ratio **(Figure 3B-C, Sup. Fig. 5)**. With excess polycation (K100:D100 ratio of 3:1), coacervate droplets have a more positive zeta potential (+26 ± 1 mV). Protein assemblies were observed at the interface, differing somewhat from the assemblies at the 1:1 K100:D100 ratio in that the interfacial protein coatings did not fully conform to the curved surfaces of the droplets and were also found projecting into the droplet interiors **(Figure 3B)**. In contrast, at a K100:D100 ratio of 1:3, where excess polyanion resulted in coacervate droplets with negative surface charge (zeta potential = –19 ± 1 mV), BMC shell protein coatings were not at the interface. Instead, aggregates of the shell proteins were observed in the dilute continuous phase **(Figure 3C)**. Both BMC-H samples behaved similarly in each K100/D100 charge ratio tested **(Figure 3, Sup. Fig. 5B-D)**. Furthermore, imaging the droplets qualitatively suggested that shell protein coatings may stabilize droplet number over time **(Sup. Fig. 7)**. As was observed in the PEG/dextran system, interfacial assembly was sensitive to the molar ratio of Sulfo-Cy3 labeling to BMC shell protein **(Sup. Fig. 8)**. Interfacial

coatings' uniformity and completeness were variable from preparation to preparation due to a size distribution of shell protein assemblies in solution, which we attribute in part to pre-existing shell protein assemblies in protein stocks and in part to newly-formed assemblies/aggregates in coacervate samples (discussed in the next section). Overall, these observations support a charge-based assembly mechanism for BMC shell protein coatings at the K100/D100 coacervate surface.

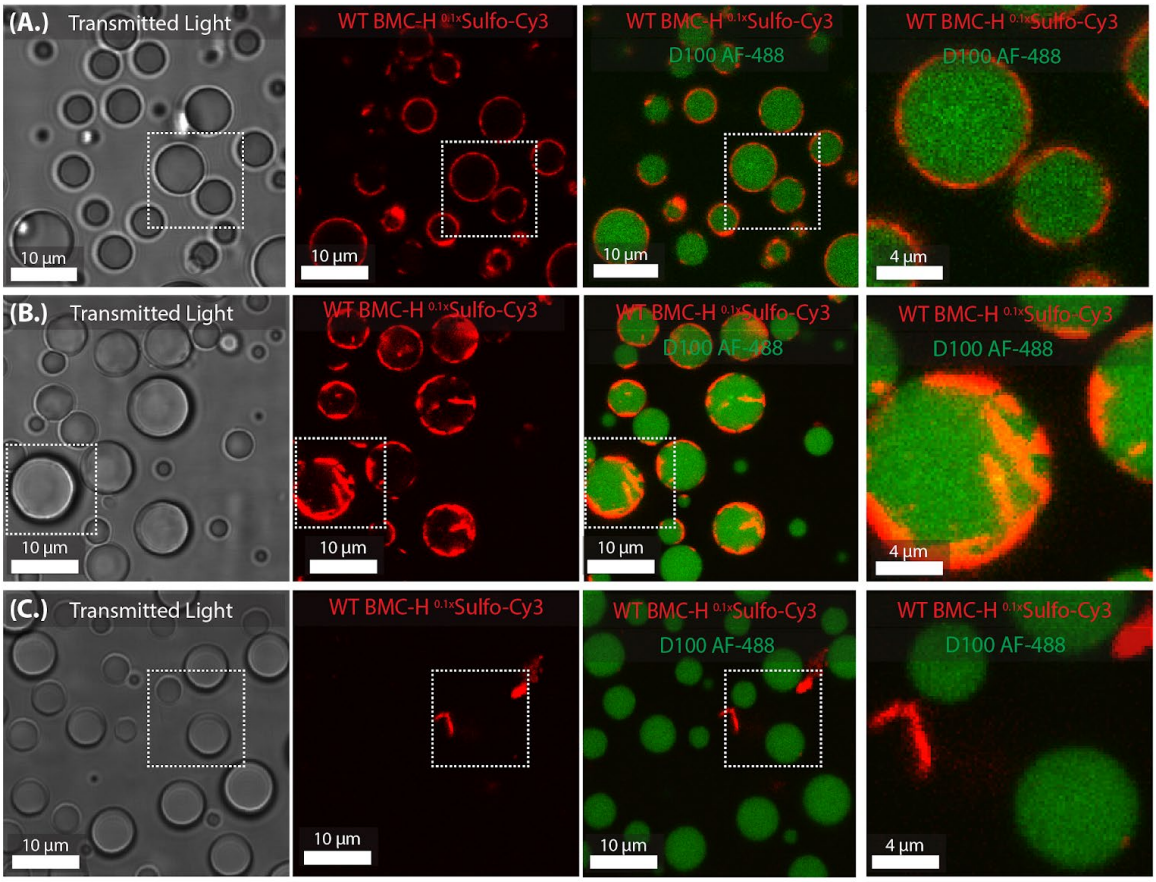

Figure 3: BMC-H$_{wt}$ hexamers coat the surface of coacervates as a function of polyelectrolyte charge (A) – (C) Confocal fluorescence microscopy of mixed droplets and labeled BMC$_{wt}$ shell protein (A) 0.05 mM K100 and 0.05 mM D100 (+19 mV ± 1). (B) 0.075 mM K100 and 0.025 mM D100 (+26 mV ± 1). (C) 0.025 mM K100 and 0.075 mM D100 (-19 mV ± 1). Fluorescence channels have been intensity-adjusted for ease of visualization and false-colored (green for D100 labeled with AF-488 and red for Sulfo-Cy3-labeled shell proteins). All

samples are in n 20 mM Tris-HCl, 50 mM NaCl, 10 mM $MgCl_2$, pH 8.0 buffer with ~0.1 mg/mL protein. Images depicted represent trends observed for at least three biological replicates.

K100 in the dilute phase of K100/D100 coacervates influences BMC shell protein aggregation.

In complex coacervate systems, although both polycations and polyanions are concentrated into the coacervate phase, some polyelectrolytes nevertheless remain in the dilute phase at equilibrium.[79,80] These dilute phase polyelectrolytes have been shown to influence interfacial liposome assembly.[81] We hypothesized that excess K100 could be interacting with the negatively charged BMC shell proteins in the dilute phase prior to the liquid/liquid interface. To test for this possibility, we added labeled shell proteins to samples of dilute phase from which coacervates had been removed via centrifugation, and to buffered solutions of the individual polypeptides. Protein assembly in these solutions was investigated by confocal fluorescence microscopy and negative stain electron microscopy **(Figure 4, Sup. Fig. 9-12, Sup. Mov. 1)**. Confocal microscopy imaging of the larger assemblies from K100-containing samples showed colocalization of Cy3-labeled BMC-H proteins with AF-488-labeled K100 (**Sup. Fig. 9**). These assemblies were largely anisotropic, with irregular shapes consistent with stacked sheets and/or long rod-like shapes. Cy3-labeled BMC-H_{K28A} also formed micron-sized assemblies in the dilute phase of a K100/D100 coacervate (**Sup. Mov. 1**). The role of K100 in forming these large aggregates was further supported by observing how the order of addition of polyelectrolytes affected the interfacial assembly of proteins in coacervates (**Sup. Fig. 10**). Generally, coacervates were prepared by mixing K100 and D100 before addition of protein, a process that in principle allows the anionic D100 to largely saturate the cationic K100 binding sites prior to adding the shell proteins. However, when a shell protein sample was added after K100, but before D100, distinct fibril or rolled lattice assemblies were observed **(Sup. Fig. 10A)**, which were not observed when protein was added followed by D100 and then K100 **(Sup. Fig. 10B)**. Transmission electron microscopy of Cy3-labeled BMC-H_{wt} found samples assembled into relatively flat sheets on electron microscopy grids (**Fig. 4A, Sup. Fig 2, Sup. Fig. 11A**), while samples incubated in a buffer with K100 produced more 3-D stacking and more prominent delineation of the hexamer protein outline (**Fig. 4B, Sup. Fig. 11B-C**). The Fourier transform of the TEM images of both control and K100 supplemented samples contained hexagonal

symmetry, but the latter had multi-layered orientations. Confocal fluorescence microscopy images of the dilute phase of an excess polycation coacervate sample showed the colocalization of dilute phase K100 (labeled with AF-488) with the fluorescent signal of Sulfo-Cy3-labeled shell proteins (**Fig. 4C**). These data indicate that polylysine in the dilute continuous phase favors BMC shell protein association in solution which in turn impacts protein shell formation around coacervate droplets.

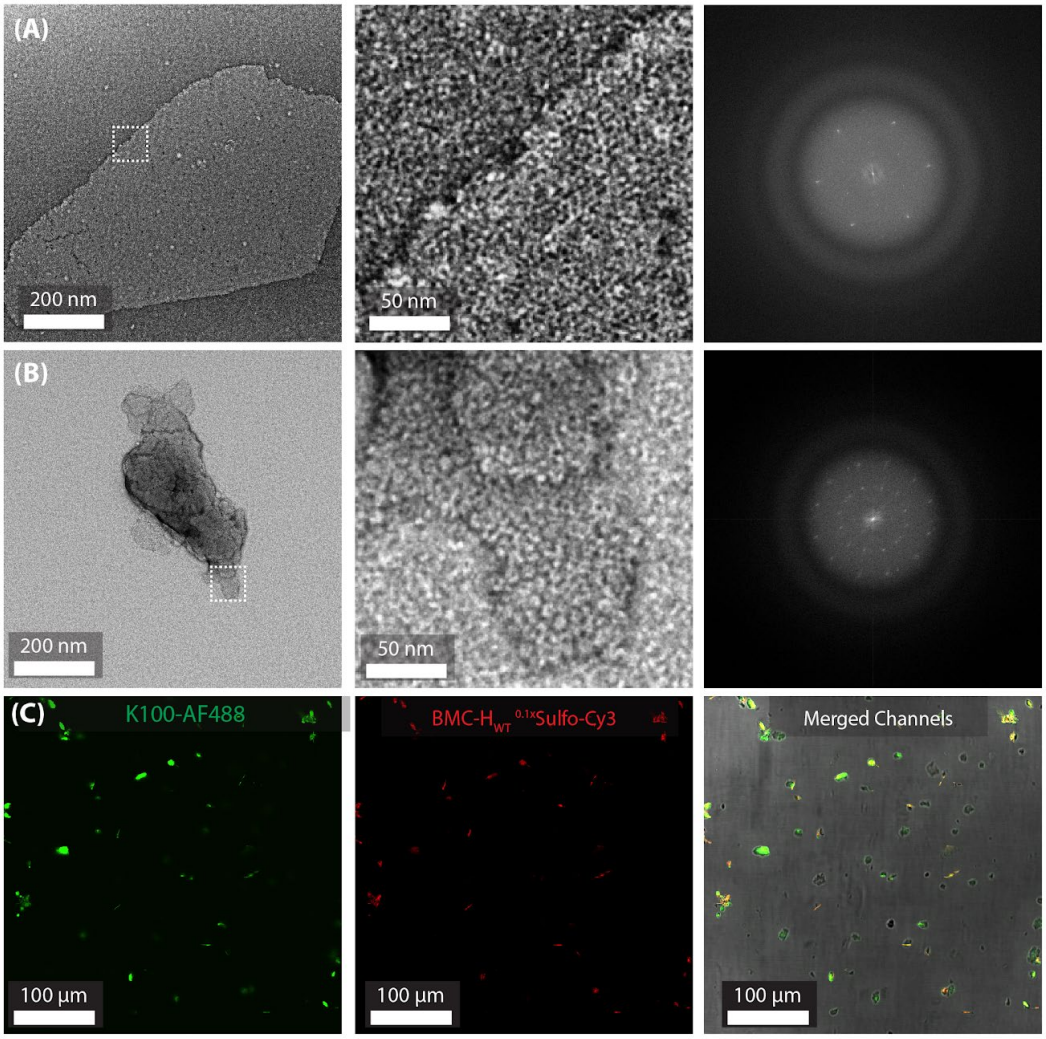

Figure 4: BMC-H$_{wt}$ shell protein lattice assembly influenced by K100 in solution. (A) - (B) TEM negative stain of 0.1 mg/mL BMC-H$_{wt}$ protein in 20 mM Tris-HCl, 50 mM NaCl, 10 mM MgCl2, pH 8.0 buffer. Left and middle panels show different magnification with the boxed areas on the left magnified in middle panels. The far-right panel is a Fourier transform of the boxed area. (A) BMC-H$_{wt}$ protein in buffer (B) BMC-H$_{wt}$ protein in buffer with 0.05 mM K100 (C)

Dilute phase confocal fluorescence microscopy images from 0.075 mM K100 and 0.025 mM D100 coacervate solution with BMC-H_{wt}-Sulfo-Cy3 at 0.1 mg/mL. Fluorescence channels have been intensity-adjusted for ease of visualization and false-colored (green for K100 labeled with AF-488 and red for Sulfo-Cy3-labeled shell proteins). Images depicted represent trends observed for at least three biological replicates.

BMC shell protein coatings around complex coacervates is compatible with biomolecular cargo and alternative coacervate polyions.

A feature of complex coacervate droplets as model organelles or protocells is their ability to concentrate biomolecular cargo such as enzymes and nucleic acids.[46,77,82] We therefore tested whether biomolecular cargo could be encapsulated within the K100/D100 coacervate without interfering with shell protein coating around the coacervate. We chose commonly encapsulated biomolecules: the enzyme glucose oxidase (GOx) and a model nucleic acid polyuridylic acid (U45).[83,84] Fluorescently-labeled GOx or U45 was added during coacervate formation at 1:1 K100:D100 charge ratio with Sulfo-Cy3 labeled BMC shell proteins (**Figure 5A-B, Sup. Fig. 12A-B**). Both GOx and U45 were found to accumulate strongly in the K100/D100 droplets and interfacial assembly of BMC shell protein coatings appeared similar to samples lacking biomolecular cargo. We then tested the activity of the loaded biomolecular cargo by performing a coupled enzyme reaction with GOx and horseradish peroxidase (HRP) (**Sup. Fig. 12C**). In this reaction, a fluorescently detectable product, resorufin, is formed from the coupled enzymes and substrates. After mixing enzymes, polyelectrolytes then Sulfo-Cy3 BMC shell proteins, coacervates with BMC shell protein coatings were observed on the microscope slide. Upon the addition of Amplex Red and glucose, a rapid increase in fluorescence occurred inside the droplet due to fluorescent product generation whereas no change in fluorescence was observed in the absence of GOx; this indicates retention of both enzymes' activity. (**Figure 5C-D**, **Sup. Fig. 12D**).

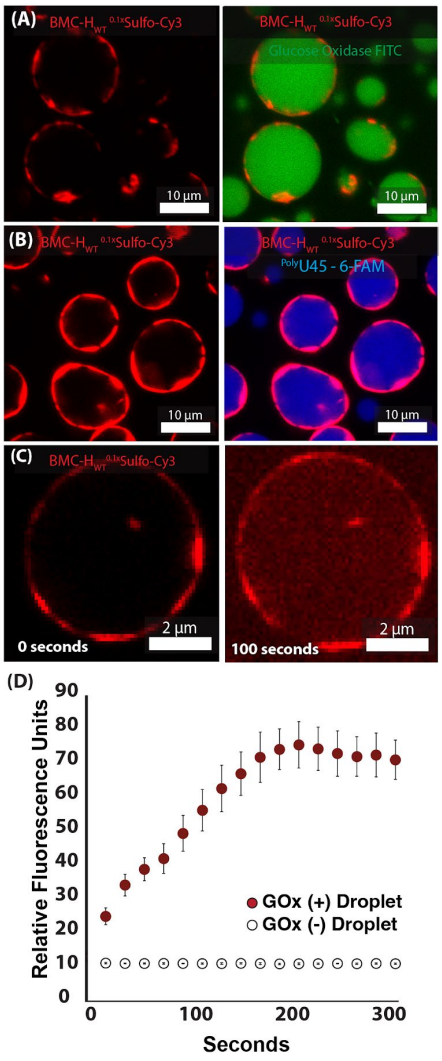

Figure 5: Biomolecule cargo incorporation into BMC-H_{wt} Shell Protein/K100/D100 coacervate mixtures (A) - (B) Confocal fluorescence microscopy of mixed K100/D100 droplets, labeled biomolecular cargo, and labeled BMC_{wt} shell protein (A) Glucose oxidase FITC. (B) Polyuridylic acid 45-mer 6-FAM. (C) Representative confocal fluorescence microscopy images showing increased fluorescence intensity in a BMC-H_{wt} shell protein/K100/D100 droplet at times 0 and 100 s after glucose addition due to resorufin production by the GOx-HRP coupled enzymatic reaction. (D) Average measured relative fluorescence over time in five representative K100/D100 droplets with BMC-H_{wt} coatings. All samples are in 20 mM Tris-HCl, 50 mM NaCl, 10 mM $MgCl_2$, pH 8.0 buffer with 0.1 mg/mL shell protein. Fluorescence channels have been intensity-adjusted for ease of visualization and false-colored (green for GOx labeled with FITC, blue for U45 labeled with 6-FAM, and red for

Sulfo-Cy3-labeled shell proteins and resorufin fluorescence; panels in part (C) have been intensity-adjusted identically for comparison). Images depicted represent trends observed for at least three biological replicates.

Droplet formation by complex coacervation is possible for a wide range of biological and nonbiological polyelectrolytes. The choice of which polyelectrolytes to use can depend on factors including cost and compatibility with cargo encapsulation and/or retention of catalytic activity.[82,85,86] To determine whether BMC shell protein droplet interface coating was compatible with other complex coacervate compositions, we chose two representative polyion pairs: the biomolecule-based K100/ATP system and the synthetic polymer poly-diallyldimethylammonium (PDADMA, 8100 MW) and poly-acrylic acid (PAA, 5100 MW) system. Based on the findings described in the previous section, these coacervate systems were chosen to have longer polycations than polyanions, which is expected to yield positively charged droplets with a higher concentration of anionic rather than cationic species in the dilute phase due to the greater translational entropy of the shorter polyions.[87,88] Images showing BMC-H_{wt} coatings around K100/ATP droplets that have Alexa-647 labeled HRP cargo can be seen in **Sup. Fig 13A-B**. When the enzymatic reaction was initiated by adding hydrogen peroxide and Amplex Red, an increase in resorufin signal was observed (**Sup. Fig 13C-D**). We were also able to coat PDADMA/PAA coacervate droplets with BMC shell proteins (**Sup. Fig. 14**). The PDADMA/PAA system is well-studied and can be readily prepared in larger volumes as compared to the biomolecule-based systems. Here, we incorporated several fluorescently-labeled enzymes with different isoelectric points within the coacervate droplets and observed the formation of BMC-H_{wt} coatings around droplets containing fluorescently-labeled glucose oxidase, horseradish peroxidase, or alkaline phosphatase (**Sup. Fig. 14B-C**). These results highlight the general methodology of using BMC shell protein to coat complex coacervate droplets and house biomolecular cargo(s).

BMC shell protein interface coating in combined K100/D100 + PEG/dextran aqueous three-phase system.

We then combined the PEG/dextran and K100/D100 LLPS systems together and examined BMC-H shell protein interface assembly in a multiphase system. When K100/D100 coacervates are mixed with a PEG/dextran ATPS, a multiphase system emerges in which K100/D100 coacervate droplets reside within larger dextran-rich phase droplets, which are in turn surrounded by a PEG-rich continuous phase (**Figure 1D-E)**. This morphology, a result of minimizing system energy, suggests that interfacial tension between the PEG-rich and dextran-rich phases is lower than that between the other possible interfaces, and that contact between the coacervates and the PEG-rich phase would be the most energetically unfavorable. Similar multi-phase morphologies for coacervates within dextran-rich droplets have been reported for Ca^{2+}/polyaspartate coacervates, in which the multiphase organization was used to control local microenvironments during bioinspired mineralization.[89] Therein, nanoscale lipid vesicles were assembled at the outer interface of the dextran-rich droplets and the dextran/coacervate interface remained uncoated. In contrast, we observed BMC shell protein lattices assembling around the K100/D100 coacervates in the multiphase droplets at a 1:1 charge ratio (**Figure 6A-C, Sup. Fig. 15-16)**. Since the PEG/dextran system contains only neutral polymers, we reasoned that the charge-based tunability of BMC shell protein lattice assembly seen in coacervate systems (**Fig. 3**) may still apply in the multiphase systems. An excess polyanion coacervate droplet (1:3 charge ratio of K100:D100) in a three-phase system influences labeled BMC shell proteins localized to the interface between the dextran-rich and PEG-rich phases **(Figure 6D, Sup. Fig. 15-16)**. This supports repulsive interactions between shell proteins and interior droplet coacervate, presumably due to shared negative charges. As in the two-phase coacervate droplet system, when the system shifts from 1:1 polyelectrolyte ratio to an excess polycation coacervate (3:1 charge ratio of K100:D100), labeled proteins integrate into coacervate droplet phase **(Figure 6E, Sup. Fig. 15-16)**. These results support that the polyelectrolyte charge ratio can tune the location of BMC-H shell proteins in an aqueous three-phase system without re-optimization despite likely changes in the absolute compositions of all of the phases due to their coexistence and re-equilibration.

Conclusion:

Here, we demonstrate that all-aqueous LLPS droplets can serve as templates for assemblies of BMC shell proteins. Observation of protein shell self-assembly around droplets in four separate all-aqueous systems (PEG/dextran, K100/D100, PDADMA/PAA, and K100/ATP) suggests this is a general approach. The resulting protein coatings served as physical barriers against coacervate droplet coalescence, while still allowing molecular transport of enzyme substrates/products. When multiple interfaces were present, it was possible to direct BMC shell protein lattice assembly to either the K100/D100 ("organelle") or PEG/dextran ("cytoplasm") interface by adjusting the K100:D100 charge ratio, and hence droplet surface charge, to attract or repel negatively charged BMC-H proteins. These results set the stage for further control over BMC shell protein coatings at selected interfaces in increasingly complex scenarios, where interfaces are present between multiple coexisting liquid phases, as in biological cells. Additional study robustly defining environmental factors and the dynamics to shell protein assembly at interfaces, in bulk, or in a droplet's interior will provide not only insight to synthetic cell and LLPS droplet boundary design, but also provide descriptions for how molecular crowding and LLPS influences protein self-assembly.[90–92]

BMC-H shell protein coatings differ from previously studied LLPS droplet membranes.[56,62,81,93,94] BMC-H shell protein assembly into extended 2-D arrays is dictated by protein-protein interface shape complementarity and is influenced by protein concentration and solution composition.[21,95–99] The 2D lattices formed by BMC shell proteins are appealing as functional coatings for LLPS-based interiors. More than 40,000 BMC shell proteins have been bioinformatically classified—these differ in permeability properties, surface charge, and the relative propensity for self-assembly.[14,100] Protein engineering has also modified BMC shell proteins for specific functions.[101,102] For example, introducing natural and/or engineered metal-ion coordinating BMC shell proteins could facilitate electron transfer,[103–105] while BMC shell proteins with assembly protecting groups could enable protease responsive membrane formation,[20] and those with protein-protein adaptor domains would allow cargo scaffolding.[61,106,107] Understanding the dynamics of shell protein exchange in BMC shell protein systems will prove important for future studies.

In the context of engineering synthetic BMCs, the templating of shell proteins on coacervates and ATPS systems promises to allow construction of larger shell systems—tens-of-microns — compared to the 20 nm to ~1.8 μm range currently achieved so far.[26,108] Moreover, the ability to combine BMC shell proteins with LLPS systems points to the potential for developing micron scale synthetic BMC shells with distinct permeabilities, internal solvent properties, microenvironments, and pre-loaded cargos. Although under currently studied conditions, our selected BMC shell proteins may not completely cover a droplet's surface, incomplete coatings still may alter molecular diffusion and surface exchange as evidenced by cellular condensates stabilized by other interfacial protein clusters.[109] The findings presented here provide a foundation for future efforts to establish BMC shell proteins as "proteo-membranes" for engineered microscale organelles and cells with sequence-encodable properties.

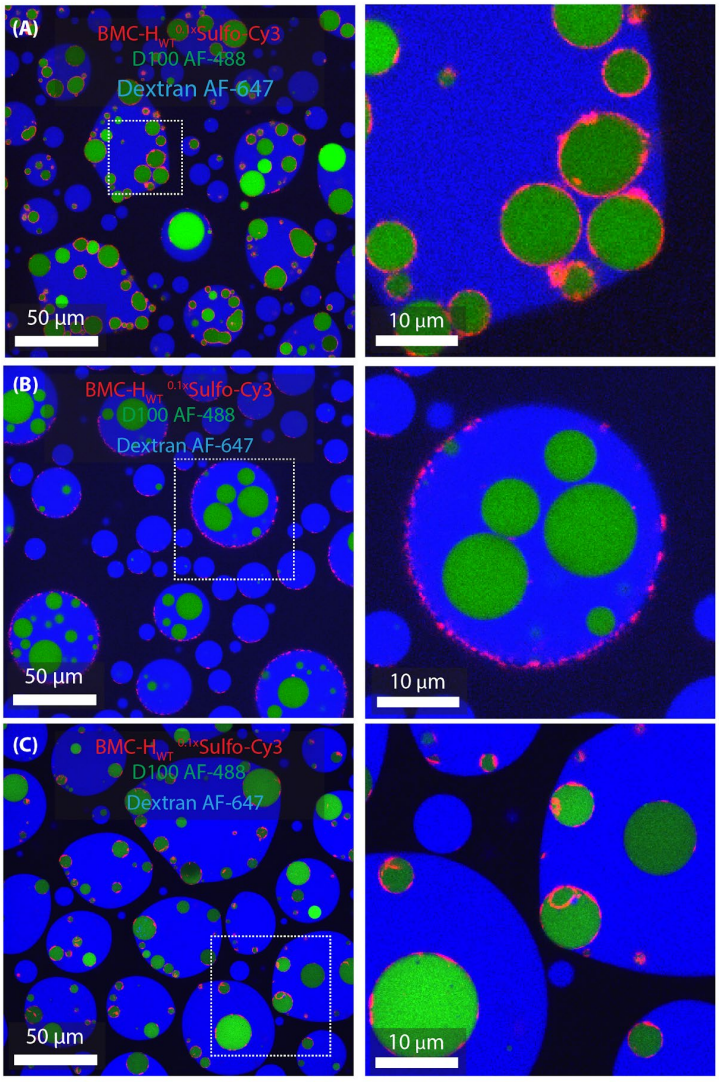

Figure 6: BMC-H$_{wt}$ shell protein assembly around coacervates-in-dextran droplets aqueous multiphase system as a function of polyelectrolyte charge ratio. Confocal fluorescence microscopy images for samples with: (A) Equal charge (0.050 mM for both K100 and D100), (B) Excess polyanion (0.025 mM K100 and 0.075 mM D100), (C) Excess polycation (0.075 mM K100 and 0.025 mM D100). Left and right panels show different magnification, with boxed areas on left magnified in right hand panels. All samples are in 20 mM Tris-HCl, 50 mM NaCl, 10 mM $MgCl_2$, pH 8.0 buffer with PEG 8kDa/dextran 10kDa ATPS solution (9:1 PEG-rich: dex-rich phase volume of an ATPS stock having 10 wt/wt% each polymer) and 0.1 mg/mL protein. Fluorescence channels have been intensity-adjusted for ease of visualization and false-colored (blue for dextran labeled with Alexa-647, green for D100 labeled with AF-488 and red for Sulfo-

Cy3-labeled shell proteins). Images depicted represent trends observed for at least three biological replicates.

Materials and Methods

Materials:

PEG 8 kDa, dextran 10 kDa, polyacrylic acid (5100 MW), glucose oxidase, horseradish peroxidase, and alkaline phosphatase were purchased from Sigma Chemical Co. (St. Louis, MO). Poly(L-aspartic acid sodium salt) 14 kDa and poly(L-lysine hydrochloride) 16 kDa were purchased from Alamanda Polymers, Inc. (Huntsville, AL). Alexa Fluor 488 hydrazide, Alexa Fluor 647 and Sulfo-Cy3 were purchased from Thermo Fisher Scientific, Co. (Waltham, MA). Poly-diallyldimethylammonium (PDADMA, 8100 MW) was purchased from Polysciences, Inc. (Warrington, PA). Silicone spacers (diameter, depth) from Electron Microscopy Sciences (Hatfield, PA) and micro cover glasses (no. 1.5, 24 x 30 mm) from VWR (West Chester, PA) were used for confocal microscopy imaging. Glass slides were silanized using N-(triethyoxysilylpropyl)-o-polyethylene oxide urethane prior to use to make the surface hydrophobic and prevent the formation of non-spherical coacervate droplets.[110] Chemicals were used as received.

Methods:

Expression, Purification, and Dye Functionalization of BMC Shell Proteins

E. coli T7 Express BL21 (DE3) cells were transformed with ~1 ng of plasmid pEJY001 or pEJY003. After overnight growth on antibiotic resistance plates, single colonies were transferred to 5 mL liquid media plus antibiotic starters for large scale batch growth. Following confluent overnight growth in starter cultures, liquid cultures were stepped up to 1 L LB media with 100 mg/mL antibiotic supplemented. 1 L cultures were grown until OD600 0.6 to 0.8 at 30˚C and then induced with 100 uM IPTG for ~16 hours of growth at 22˚C. Cell pellets were created via centrifugation of cultures and stored at -20˚C. Frozen pellets were then resuspended with 20 mL of 50 mM Tris-HCl, 100 mM NaCl, and 10 mM $MgCl_2$ pH 8.0 (Resuspension Buffer) supplemented with lysozyme (~5 mg total), DNAase (~0.2 mg total), and RNAase (~0.2 mg total). French press treatment at 1,500 PSI then ruptured the cells. Triton X-100 was then added to the cell lysis solution at a final concentration of 1%, allowed to mix for 10 minutes, then

fractionated via centrifugation at 20,000*g* for 20 minutes. The insoluble protein pellet containing the higher-order assembly of shell proteins was then washed with 30 mL 1% Triton X-100 Resuspension Buffer for a total of 3 rounds with centrifugation separating the pellet and fresh solution added with each round. A single round of resuspending the pellet in 500 mM NaCl modified Resuspension Buffer helped improve pellet quality. Protein pellets were then washed an additional time in Resuspension Buffer, followed by a single wash in dH20, and then stored in Resuspension Buffer supplemented with 0.01% sodium azide. Purified shell proteins were then buffer exchanged via centrifugation to 0.1 M sodium phosphate with 0.05 sodium chloride buffer at pH 8.0. Protein concentration was determined with a Nanodrop UV-Vis instrument (Thermo Fisher) via measuring the absorbance at 280 nm with a calculated protein absorbance 1% value of 2.95. Approximately 2.5 μM of shell proteins was mixed from an 80 mM sulfo-Cyanine 3 NHS-ester dissolved in water (Lumiprobe). Following overnight incubation at 4˚C, excess dye was removed via centrifugation and fresh 0.1 M sodium phosphate buffer addition. Once excess dye appeared removed (~3x washes), the brightly pink colored protein pellets were transferred to 20 mM Tris-HCl, 50 mM NaCl, 10 mM $MgCl_2$ pH 8.0. SDS-PAGE protein analysis utilized 4-20% Mini-PROTEAN TGX precast gels (BioRad). A 0.6% agarose gel (TopVision, ThermoFischer) was used for the dye concentration BMC-H_{wt} migration experiment.

Formation of PEG/dextran ATPS: All ATPS stocks were prepared at 10g total mass: 10%/10% w/w by dissolving 1.000g of PEG (8 kDa), 1.000g of dextran (10 kDa) in 8.000g of 20 mM Tris buffer pH 8.0, 50 mM NaCl and 10 mM $MgCl_2$. Buffer was prepared using a combination of Tris hydrochloride and Tris base. Polymers were dissolved by stirring the mixture for 1 hour. The two phases were allowed to equilibrate overnight at 5 °C, and then were separated via pipet. The PEG-rich phase and dextran-rich phase from this system were mixed back together for all subsequent sample preparations.[111,112] Each ATPS had a 1:9 volume ratio of dextran-rich to PEG-rich phases. Dextran-rich phase in each sample was equilibrated with Alexa-647 labeled dextran (10:1 non-labeled: labeled) for imaging.

Formation of BMC shell protein coated K100/D100 coacervates: Coacervate samples were prepared in 20 mM Tris buffer pH 8.0, 50 mM NaCl and 10 mM $MgCl_2$ at polypeptide charge concentrations (charge concentration = charge per molecule x concentration) ranging from 5 mM

to 7.5 mM. BMC shell protein coated coacervates were achieved with the following order of addition: buffer with salts, a polyelectrolyte (i.e., either K100 or D100) equilibrated with the same Alexa-488 labeled polyelectrolyte (10:1 non-labeled: labeled), the oppositely charged unlabeled polyelectrolyte, and Sulfo-Cy3-labeled BMC shell proteins followed by gentle mixing via pipet.

TEM negative stain of BMC shell proteins mixed with K100: Droplets of 10 μL protein samples (~0.1 mg-mL) in 20 mM Tris-HCl (pH 8.0), 50 mM NaCl and 10 mM $MgCl_2$ alone or buffer supplemented with 0.05 mM K100 were placed on parafilm. 300-mesh copper electron microscopy grids (Ted Pella) were then floated on droplets for five minutes. Samples were transferred to a water droplet for 1 minute. The grids then were transferred to a filtered 1% uranyl acetate droplet for five minutes and then transferred to a water droplet for another one minute. Samples were imaged on a Zeiss Libra I20 electron microscope equipped with a Gatan Ultrascan CCD camera.

Formation of BMC shell protein coated PDADMA/polyacrylic acid coacervates: Coacervate samples were prepared in 20 mM Tris buffer pH 8.0, 50 mM NaCl, and 10 mM $MgCl_2$ at a polymer charge concentration of 15 mM. BMC shell protein coated coacervates were achieved with the following order of addition: buffer with salts, PDDA (MW 8100), polyacrylic acid (MW 5100), and Sulfo-Cy3-labeled BMC shell proteins followed by gentle mixing via pipet.

Formation of BMC shell protein coated K100/ATP coacervates: Coacervate samples were prepared in 20 mM Tris buffer pH 8.0, 50 mM NaCl and 10 mM $MgCl_2$ at a charge concentration of 5 mM. BMC shell protein coated coacervates were achieved with the following order of addition: buffer with salts, K100, ATP, and Sulfo-Cy3-labeled BMC shell proteins followed by gentle mixing via pipet.

Formation of aqueous three phase systems: Aqueous three phase systems consisting of a K100/D100 coacervate phase residing in a dextran-rich phase surrounded by a PEG-rich phase were prepared by adding the polymers in the following order: D100 equilibrated with Alexa-488

labeled D100 (10:1 non-labeled: labeled), K100, dextran rich phase equilibrated with Alexa-647 labeled dextran (10:1 non-labeled: labeled), and PEG rich phase followed by pipet mixing.

Biomolecular cargo encapsulation and enzyme activity: Fluorescently labeled biomolecules (enzymes/RNA) were added to prepared coacervate samples and their partitioning behavior was observed on the confocal microscope. In order to monitor the enzyme activity, glucose oxidase and horseradish peroxidase were mixed with coacervates then with BMC shell proteins, and fluorescent product generation was monitored upon the addition of Amplex Red and glucose.

Confocal imaging: Samples were deposited on a silanized glass slide with a spacer and coverslip and imaged within 5 minutes of preparation. Imaging was done at room temperature (25°C). Confocal microscopy images were collected with an excitation at 633 nm for Alexa 647-labeled dextran, 488 nm for Alexa 488-labeled D100 or K100 and 532 nm for Sulfo-Cy3-labeled BMC-H proteins using a Leica TCS SP5 PL confocal microscope using a 63 x1.4 NA APO objective.

Image Analysis, and Figure Preparation

Image analysis used software ImageJ (Fiji.net). Microsoft Excel (Microsoft), Numbers (Apple), Igor Pro (Wavemetrics), and Adobe Illustrator (Adobe) organized data, prepared graphs, calculated statistics, and designed figures. Fluorescence intensities for the distribution of Cy3 labeled BMC- H_{wt} shell proteins between interface, exterior continuous phase, and droplet interior were averaged by analyzing intensity profiles derived from line scans (1 per droplet) drawn across 10 droplets each from 3 separate confocal microscopic images. For PEG/dextran ATPS, line scans were taken across the fractions of interface (~40%) that had visible BMC- H_{wt} shell proteins assembled. Microsoft Excel and IgorPro calculated statistics including mean, median, standard deviation, and p values.

Acknowledgements

D.T.A and E.J.Y contributed equally to this work. E.J.Y and C.A.K were supported by the National Science Foundation under award number EF-1935047. D.T.A, A.T.R and C.D.K were

supported by the National Science Foundation under award number EF-1935059. L.C.D, S.U, and M.O.S were supported by the National Science Foundation under award number EF-1935049.

Conflicts of Interest

The authors declare no conflicts of interest.

References:

[1] S. Mann, *Acc. Chem. Res.* **2012**, *45*, 2131.
[2] P.-A. Monnard, P. Walde, *Life* **2015**, *5*, 1239.
[3] C. A. Azaldegui, A. G. Vecchiarelli, J. S. Biteen, *Biophysical Journal* **2021**, *120*, 1123.
[4] C. D. Crowe, C. D. Keating, *Interface Focus.* **2018**, *8*, 20180032.
[5] C. A. Kerfeld, C. Aussignargues, J. Zarzycki, F. Cai, M. Sutter, *Nat. Rev. Microbiol.* **2018**, *16*, 277.
[6] L. Schoonen, J. C. M. Van Hest, *Adv. Mater.* **2016**, *28*, 1109.
[7] N. J. Gaut, K. P. Adamala, *Advanced Biology* **2021**, *5*, 2000188.
[8] C. Guindani, L. C. da Silva, S. Cao, T. Ivanov, K. Landfester, *Angew Chem Int Ed* **2022**, *61*, DOI 10.1002/anie.202110855.
[9] D. Di Iorio, S. V. Wegner, *Current Opinion in Chemical Biology* **2022**, *68*, 102145.
[10] D. Gaur, N. C. Dubey, B. P. Tripathi, *Advances in Colloid and Interface Science* **2022**, *299*, 102566.
[11] E. Bailoni, M. Partipilo, J. Coenradij, D. A. J. Grundel, D. J. Slotboom, B. Poolman, *ACS Synth. Biol.* **2023**, acssynbio.3c00062.
[12] N. Martin, *ChemBioChem* **2019**, *20*, 2553.
[13] S. Shil, M. Tsuruta, K. Kawauchi, D. Miyoshi, *BioTech* **2023**, *12*, 26.
[14] M. Sutter, M. R. Melnicki, F. Schulz, T. Woyke, C. A. Kerfeld, *Nat Commun* **2021**, *12*, 3809.
[15] C. A. Kerfeld, M. R. Sawaya, S. Tanaka, C. V. Nguyen, M. Phillips, M. Beeby, T. O. Yeates, *Science* **2005**, *309*, 936.
[16] M. G. Klein, P. Zwart, S. C. Bagby, F. Cai, S. W. Chisholm, S. Heinhorst, G. C. Cannon, C. A. Kerfeld, *Journal of Molecular Biology* **2009**, *392*, 319.
[17] S. Tanaka, C. A. Kerfeld, M. R. Sawaya, F. Cai, S. Heinhorst, G. C. Cannon, T. O. Yeates, *Science* **2008**, *319*, 1083.
[18] J. K. Lassila, S. L. Bernstein, J. N. Kinney, S. D. Axen, C. A. Kerfeld, *Journal of Molecular Biology* **2014**, *426*, 2217.
[19] F. Cai, S. L. Bernstein, S. C. Wilson, C. A. Kerfeld, *Plant Physiology* **2016**, *170*, 1868.
[20] A. R. Hagen, J. S. Plegaria, N. Sloan, B. Ferlez, C. Aussignargues, R. Burton, C. A. Kerfeld, *Nano Lett.* **2018**, *18*, 7030.
[21] M. Sutter, M. Faulkner, C. Aussignargues, B. C. Paasch, S. Barrett, C. A. Kerfeld, L.-N. Liu, *Nano Lett.* **2016**, *16*, 1590.
[22] M. Sutter, T. G. Laughlin, N. B. Sloan, D. Serwas, K. M. Davies, C. A. Kerfeld, *Plant Physiol.* **2019**, *181*, 1050.

[23] L. Liu, *Microbial Biotechnology* **2021**, *14*, 88.
[24] E. E. Cesle, A. Filimonenko, K. Tars, G. Kalnins, *Protein Science* **2021**, *30*, 1035.
[25] Y. Q. Tan, S. Ali, B. Xue, W. Z. Teo, L. H. Ling, M. K. Go, H. Lv, R. C. Robinson, A. Narita, W. S. Yew, *Biomacromolecules* **2021**, *22*, 4095.
[26] B. H. Ferlez, H. Kirst, B. J. Greber, E. Nogales, M. Sutter, C. A. Kerfeld, *Advanced Materials* **2023**, 2212065.
[27] J. B. Parsons, S. Frank, D. Bhella, M. Liang, M. B. Prentice, D. P. Mulvihill, M. J. Warren, *Molecular Cell* **2010**, *38*, 305.
[28] N. K. Bari, G. Kumar, J. P. Hazra, S. Kaur, S. Sinha, *J. Mater. Chem. B* **2020**, *8*, 523.
[29] G. M. Rotskoff, P. L. Geissler, *Proc. Natl. Acad. Sci. U.S.A.* **2018**, *115*, 6341.
[30] F. Mohajerani, M. F. Hagan, *PLoS Comput Biol* **2018**, *14*, e1006351.
[31] F. Mohajerani, E. Sayer, C. Neil, K. Inlow, M. F. Hagan, *ACS Nano* **2021**, *15*, 4197.
[32] J. Douliez, A. Perro, L. Béven, *ChemBioChem* **2019**, *20*, 2546.
[33] Y. Chao, H. C. Shum, *Chem. Soc. Rev.* **2020**, *49*, 114.
[34] J. Esquena, *Current Opinion in Food Science* **2023**, *51*, 101010.
[35] N. Gao, S. Mann, *Acc. Chem. Res.* **2023**, *56*, 297.
[36] Z. Lin, T. Beneyton, J. Baret, N. Martin, *Small Methods* **2023**, 2300496.
[37] F. Pir Cakmak, A. M. Marianelli, C. D. Keating, *Langmuir* **2021**, *37*, 10366.
[38] Y. Zhang, Y. Chen, X. Yang, X. He, M. Li, S. Liu, K. Wang, J. Liu, S. Mann, *J. Am. Chem. Soc.* **2021**, *143*, 2866.
[39] N. Coudon, L. Navailles, F. Nallet, I. Ly, A. Bentaleb, J.-P. Chapel, L. Béven, J.-P. Douliez, N. Martin, *J. Colloid Interface Sci.* **2022**, *617*, 257.
[40] N. Gao, C. Xu, Z. Yin, M. Li, S. Mann, *J. Am. Chem. Soc.* **2022**, *144*, 3855.
[41] E. Dickinson, *Trends in Food Science & Technology* **2019**, *83*, 31.
[42] M. Vis, J. Opdam, I. S. J. van 't Oor, G. Soligno, R. van Roij, R. H. Tromp, B. H. Erné, *ACS Macro Lett.* **2015**, *4*, 965.
[43] D. M. A. Buzza, P. D. I. Fletcher, T. K. Georgiou, N. Ghasdian, *Langmuir* **2013**, *29*, 14804.
[44] A. F. Mason, B. C. Buddingh', D. S. Williams, J. C. M. Van Hest, *J. Am. Chem. Soc.* **2017**, *139*, 17309.
[45] M. Abbas, J. O. Law, S. N. Grellscheid, W. T. S. Huck, E. Spruijt, *Advanced Materials* **2022**, *34*, 2202913.
[46] W. J. Altenburg, N. A. Yewdall, D. F. M. Vervoort, M. H. M. E. Van Stevendaal, A. F. Mason, J. C. M. Van Hest, *Nat Commun* **2020**, *11*, 6282.
[47] Y. Ji, Y. Lin, Y. Qiao, *J. Am. Chem. Soc.* **2023**, jacs.3c01326.
[48] Z. Xu, S. Wang, C. Zhao, S. Li, X. Liu, L. Wang, M. Li, X. Huang, S. Mann, *Nat Commun* **2020**, *11*, 5985.
[49] B. T. Nguyen, T. Nicolai, L. Benyahia, *Langmuir* **2013**, *29*, 10658.
[50] X. Huang, M. Li, D. C. Green, D. S. Williams, A. J. Patil, S. Mann, *Nat Commun* **2013**, *4*, 2239.
[51] L.-H. Xue, C.-Y. Xie, S.-X. Meng, R.-X. Bai, X. Yang, Y. Wang, S. Wang, B. P. Binks, T. Guo, T. Meng, *ACS Macro Lett.* **2017**, *6*, 679.
[52] J. Li, X. Liu, L. K. E. A. Abdelmohsen, D. S. Williams, X. Huang, *Small* **2019**, *15*, 1902893.
[53] B. Monterroso, S. Zorrilla, M. Sobrinos-Sanguino, C. D. Keating, G. Rivas, *Sci Rep* **2016**, *6*, 35140.

[54] Y. Song, U. Shimanovich, T. C. T. Michaels, Q. Ma, J. Li, T. P. J. Knowles, H. C. Shum, *Nat Commun* **2016**, *7*, 12934.
[55] K. A. Ganar, L. Leijten, S. Deshpande, *ACS Synth. Biol.* **2022**, *11*, 2869.
[56] F. Fanalista, S. Deshpande, A. Lau, G. Pawlik, C. Dekker, *Adv. Biosys.* **2018**, *2*, 1800136.
[57] P.-Å. Albertsson, in *Advances in Protein Chemistry*, **1970**, pp. 309–341.
[58] C. D. Keating, *Acc. Chem. Res.* **2012**, *45*, 2114.
[59] H. G. Bungenberg de Jong, H. R. Kruyt, **1929**, pp. 849–856.
[60] N. A. Yewdall, A. A. M. André, T. Lu, E. Spruijt, *Current Opinion in Colloid & Interface Science* **2021**, *52*, 101416.
[61] E. J. Young, J. K. Sakkos, J. Huang, J. K. Wright, B. Kachel, M. Fuentes-Cabrera, C. A. Kerfeld, D. C. Ducat, *Nano Lett.* **2020**, *20*, 208.
[62] F. M. Kelley, B. Favetta, R. M. Regy, J. Mittal, B. S. Schuster, *Proc. Natl. Acad. Sci. U.S.A.* **2021**, *118*, e2109967118.
[63] D. C. Dewey, C. A. Strulson, D. N. Cacace, P. C. Bevilacqua, C. D. Keating, *Nat Commun* **2014**, *5*, 4670.
[64] R. Hans Tromp, M. Vis, B. H. Erné, E. M. Blokhuis, *J. Phys.: Condens. Matter* **2014**, *26*, 464101.
[65] F. Pir Cakmak, C. D. Keating, *Sci Rep* **2017**, *7*, 3215.
[66] F. Gebhard, J. Hartmann, S. Hardt, *Soft Matter* **2021**, *17*, 3929.
[67] K. Sarikhani, K. Jeddi, R. B. Thompson, C. B. Park, P. Chen, *Langmuir* **2015**, *31*, 5571.
[68] S. Shi, T. P. Russell, *Adv. Mater.* **2018**, *30*, 1800714.
[69] R. Aveyard, B. P. Binks, J. H. Clint, *Advances in Colloid and Interface Science* **2003**, *100–102*, 503.
[70] E. Atefi, J. A. Mann, H. Tavana, *Langmuir* **2014**, *30*, 9691.
[71] M. S. Long, A.-S. Cans, C. D. Keating, *J. Am. Chem. Soc.* **2008**, *130*, 756.
[72] B. P. Binks, T. S. Horozov, in *Colloidal Particles at Liquid Interfaces* (Eds: B.P. Binks, T.S. Horozov), Cambridge University Press, **2006**, pp. 1–74.
[73] H. Butt, K. Graf, M. Kappl, *Physics and Chemistry of Interfaces*, Wiley, **2003**.
[74] R. J. Ellis, *Trends in Biochemical Sciences* **2001**, *26*, 597.
[75] H.-X. Zhou, G. Rivas, A. P. Minton, *Annu. Rev. Biophys.* **2008**, *37*, 375.
[76] I. Kuznetsova, K. Turoverov, V. Uversky, *IJMS* **2014**, *15*, 23090.
[77] M. Abbas, W. P. Lipiński, J. Wang, E. Spruijt, *Chem. Soc. Rev.* **2021**, *50*, 3690.
[78] E. Guzmán, F. Ortega, R. G. Rubio, *Langmuir* **2022**, *38*, 13313.
[79] S. Friedowitz, J. Lou, K. P. Barker, K. Will, Y. Xia, J. Qin, *Sci. Adv.* **2021**, *7*, eabg8654.
[80] S. P. Moulik, A. K. Rakshit, A. Pan, B. Naskar, *Colloids and Interfaces* **2022**, *6*, 45.
[81] F. Pir Cakmak, A. T. Grigas, C. D. Keating, *Langmuir* **2019**, *35*, 7830.
[82] R. R. Poudyal, F. Pir Cakmak, C. D. Keating, P. C. Bevilacqua, *Biochemistry* **2018**, *57*, 2509.
[83] Y. Chen, M. Yuan, Y. Zhang, S. Liu, X. Yang, K. Wang, J. Liu, *Chem. Sci.* **2020**, *11*, 8617.
[84] H. M. Fares, A. E. Marras, J. M. Ting, M. V. Tirrell, C. D. Keating, *Nat Commun* **2020**, *11*, 5423.
[85] K. A. Black, D. Priftis, S. L. Perry, J. Yip, W. Y. Byun, M. Tirrell, *ACS Macro Lett.* **2014**, *3*, 1088.
[86] W. C. Blocher McTigue, S. L. Perry, *Small* **2020**, *16*, 1907671.

[87] J. V. D. Gucht, E. Spruijt, M. Lemmers, M. A. Cohen Stuart, *Journal of Colloid and Interface Science* **2011**, *361*, 407.
[88] L.-W. Chang, T. K. Lytle, M. Radhakrishna, J. J. Madinya, J. Vélez, C. E. Sing, S. L. Perry, *Nat Commun* **2017**, *8*, 1273.
[89] A. T. Rowland, D. N. Cacace, N. Pulati, M. L. Gulley, C. D. Keating, *Chem. Mater.* **2019**, *31*, 10243.
[90] M. F. Hagan, F. Mohajerani, *PLoS Comput Biol* **2023**, *19*, e1010652.
[91] C. Weber, T. Michaels, L. Mahadevan, *eLife* **2019**, *8*, e42315.
[92] W. Pönisch, T. C. T. Michaels, C. A. Weber, *Biophysical Journal* **2023**, *122*, 197.
[93] J. Horn, R. Kapelner, A. Obermeyer, *Polymers* **2019**, *11*, 578.
[94] W. Mu, Z. Ji, M. Zhou, J. Wu, Y. Lin, Y. Qiao, *Sci. Adv.* **2021**, *7*, eabf9000.
[95] M. Sutter, B. Greber, C. Aussignargues, C. A. Kerfeld, *Science* **2017**, *356*, 1293.
[96] M. Faulkner, L.-S. Zhao, S. Barrett, L.-N. Liu, *Nanoscale Res Lett* **2019**, *14*, 54.
[97] Y. Li, N. W. Kennedy, S. Li, C. E. Mills, D. Tullman-Ercek, M. Olvera de la Cruz, *ACS Cent. Sci.* **2021**, *7*, 658.
[98] L. F. Garcia-Alles, M. Fuentes-Cabrera, G. Truan, D. Reguera, *PLoS Comput Biol* **2023**, *19*, e1011038.
[99] L. F. Garcia-Alles, E. Lesniewska, K. Root, N. Aubry, N. Pocholle, C. I. Mendoza, E. Bourillot, K. Barylyuk, D. Pompon, R. Zenobi, D. Reguera, G. Truan, *PLoS ONE* **2017**, *12*, e0185109.
[100] M. R. Melnicki, M. Sutter, C. A. Kerfeld, *Current Opinion in Microbiology* **2021**, *63*, 1.
[101] S. Planamente, S. Frank, *Biochemical Society Transactions* **2019**, *47*, 765.
[102] C. A. Kerfeld, M. Sutter, *Current Opinion in Biotechnology* **2020**, *65*, 225.
[103] C. Aussignargues, M.-E. Pandelia, M. Sutter, J. S. Plegaria, J. Zarzycki, A. Turmo, J. Huang, D. C. Ducat, E. L. Hegg, B. R. Gibney, C. A. Kerfeld, *J. Am. Chem. Soc.* **2016**, *138*, 5262.
[104] J. Huang, B. H. Ferlez, E. J. Young, C. A. Kerfeld, D. M. Kramer, D. C. Ducat, *Front. Bioeng. Biotechnol.* **2020**, *7*, 432.
[105] J. S. Plegaria, M. D. Yates, S. M. Glaven, C. A. Kerfeld, *ACS Appl. Bio Mater.* **2020**, *3*, 685.
[106] A. Hagen, M. Sutter, N. Sloan, C. A. Kerfeld, *Nat Commun* **2018**, *9*, 2881.
[107] H. Kirst, B. H. Ferlez, S. N. Lindner, C. A. R. Cotton, A. Bar-Even, C. A. Kerfeld, *Proc. Natl. Acad. Sci. U.S.A.* **2022**, *119*, e2116871119.
[108] G. Kumar, S. Sinha, *Current Opinion in Microbiology* **2021**, *63*, 43.
[109] A. W. Folkmann, A. Putnam, C. F. Lee, G. Seydoux, *Science* **2021**, *373*, 1218.
[110] T. T. Razunguzwa, M. Warrier, A. T. Timperman, *Anal. Chem.* **2006**, *78*, 4326.
[111] D. N. Cacace, C. D. Keating, *J. Mater. Chem. B* **2013**, *1*, 1794.
[112] C. A. Strulson, R. C. Molden, C. D. Keating, P. C. Bevilacqua, *Nature Chem* **2012**, *4*, 941.